Published in final edited form as:
Physiol Meas. 2011 December ; 32(12): 1885–1897. doi:10.1088/0967-3334/32/12/001.

On the Shape of the Common Carotid Artery, with Implications for Blood Velocity Profiles

Amir Manbachi[1,2], **Yiemeng Hoi**[1], **Bruce A. Wasserman**[3], **Edward G. Lakatta**[4], and **David A Steinman**[1,2]

[1]Biomedical Simulation Laboratory, Department of Mechanical & Industrial Engineering, University of Toronto, Toronto, ON, Canada

[2]Institute of Biomaterials and Biomedical Engineering, University of Toronto, Toronto, ON, Canada

[3]The Russell H. Morgan Department of Radiology and Radiological Sciences, The Johns Hopkins Hospital, Baltimore, MD, USA

[4]Laboratory of Cardiovascular Science, Intramural Research Program, National Institute on Aging, NIH, Baltimore, MD, USA

Abstract

Clinical and engineering studies typically assume that the common carotid artery (CCA) is straight enough to assume fully developed flow, yet recent studies have demonstrated the presence of skewed velocity profiles. Towards elucidating the influence of mild vascular curvatures on blood flow patterns and atherosclerosis, the present study aimed to characterize the three-dimensional shape of the human CCA. The left and right carotid arteries of 28 participants (62±13 years) in the VALIDATE (Vascular Aging – The Link that Bridges Age to Atherosclerosis) study were digitally segmented from 3D contrast-enhanced magnetic resonance angiograms, from the aortic arch to the carotid bifurcation. Each CCA was divided into nominal cervical and thoracic segments, for which curvatures were estimated by least squares fitting of the respective centerlines to planar arcs. The cervical CCA had mean radius of curvature of 127 mm, corresponding to a mean lumen:curvature radius ratio of 1:50. The thoracic CCA was significantly more curved at 1:16, with the plane of curvature tilted by a mean angle of 25 degrees and rotated close to 90 degrees with respect to that of the cervical CCA. The left CCA was significantly longer and slightly more curved than the right CCA, and there was a weak but significant increase in CCA curvature with age. Computational fluid dynamic (CFD) simulations carried out for idealized CCA geometries derived from these and other measured geometric parameters demonstrated that mild cervical curvature is sufficient to prevent flow from fully developing, independent of the degree of thoracic curvature. These findings reinforce the idea that fully-developed flow may be the exception rather than the rule for the CCA, and perhaps other nominally long and straight vessels.

Keywords

carotid artery; blood velocity profile; vascular geometry; Doppler ultrasound

steinman@mie.utoronto.ca.

Disclaimer The authors have no conflicts of interest to disclose.

1. Introduction

The carotid arteries are the main conduits for blood flow from the heart to the brain. The left common carotid artery (CCA) typically arises directly from the aortic arch, the right from the brachiocephalic artery off the arch. Both eventually bifurcate into an internal carotid artery (ICA), which feeds the brain, and an external carotid artery (ECA), which feeds the rest of the head. The carotid artery bifurcation has been the subject of intensive anatomical and hemodynamic study owing to the preferential development of atherosclerosis at this site (e.g., Giddens *et al.*, 1993). Less well studied are the anatomy and hemodynamics of the CCA, a vessel which is commonly considered to be straight, or at least straight enough to rationalize the assumption of fully developed blood flow proximal to the carotid bifurcation (e.g., Carallo *et al.*, 1999).

An early case study of a healthy volunteer by Caro et al. (1992) used magnetic resonance imaging (MRI) to estimate a 1:20 curvature (i.e., ratio of lumen radius to radius of curvature) of the cervical CCA, and revealed the presence of secondary velocities characteristic of so-called Dean-type flow in a planar curved tube. A Doppler ultrasound investigation of 20 healthy volunteers of various ages reported the presence of skewed velocity profiles irrespective of age, and which were attributed to “slight” CCA curvatures (Tortoli *et al.*, 2003). Recent MRI investigations have confirmed the common finding of strongly skewed blood velocity profiles in the CCA (Sui *et al.*, 2008; Ford *et al.*, 2008).

The dynamics of blood flow in tubes having simple planar curvatures (i.e., Dean flow) are well understood; however less is known about how and why more complex, shallow curvatures of vessels like the CCA produce velocity profile skewing in some cases but not others. Ultimately, such knowledge may help explain the common finding of eccentric wall thickening at the CCA (e.g. (Boussel *et al.*, 2007)), and also overcome errors in Doppler ultrasound estimations of flow and wall shear rates (e.g., Balbis *et al.*, 2005; Krams *et al.*, 2005) which typically rely on the assumption of fully-developed flow (Pantos *et al.*, 2007). Towards this ultimate end, the aim of the present study was to conduct the first thorough survey of the geometry of the human CCA from its thoracic origins to the level of the carotid bifurcation.

2. Methods

2.1. Study Subjects and Magnetic Resonance Imaging

Data for this study were acquired from the NIA-sponsored VALIDATE (Vascular Aging - The Link That Bridges Age to Atherosclerosis) study, which aims to test the hypothesis that vascular age is an important determinant of the age-associated increase in atherosclerotic disease. Specifically, the present study focused on the community-based cohort (i.e., normal vascular aging group) recruited from Baltimore Longitudinal Study for Aging (BLSA) participants (Ferrucci, 2008). Written informed consent was obtained from all participants and approval was given by the institutional review boards.

As part of a comprehensive MRI survey of the carotid bifurcations, three-dimensional (3D) contrast-enhanced magnetic resonance angiograms (CEMRA) were acquired coronally using a centric k-space ordering, with a field-of-view encompassing the aortic arch to the circle of Willis (Figure 1a). Owing to the focus on the carotid bifurcations, surface radiofrequency coils were used, resulting in reduced signal at the CCA's thoracic origins. As a result, we considered only on those cases acquired using a 3.0 Tesla scanner (Achieva; Philips Healthcare, Best, The Netherlands), as the CCA thoracic origins were more conspicuous compared to acquisitions at 1.5 Tesla. Specifically, N=32 cases were selected for analysis, encompassing both sexes (13M:19F) and a range of ages (37–85 years; mean±stdev = 63±12

years). CEMRA acquisition parameters included: 6-cm-thick coronal slab partitioned into 1-mm slices overlapping by 0.5 mm; 33-cm field-of-view acquired with a 408 × 405 acquisition matrix zero-padded to 512 × 512; Magnevist (Bayer Schering Pharma AG, Berlin, Germany) contrast injection of 0.2 mL/kg at 2 mL/sec.

2.2. Image Segmentation and Shape Characterization

The left and right CCA lumens were digitally segmented from each 3D CEMRA series using the computer-assisted Fast Marching Level Set method of the open-source Vascular Modeling Tool-Kit (VMTK; www.vmtk.org). This requires a user to initialize the surface via interactive selection of one or more thresholds, but otherwise generates the lumen surface automatically based on the image gradients. In four cases, either the left or right CCA could not be reliably segmented down to its origin at the aortic arch or brachiocephalic trunk; these cases were excluded from further analysis, leaving 28 left/right pairs for geometric characterization. One quarter (i.e., seven) of the cases were selected randomly for re-segmentation after one year, in order to test the reproducibility of the geometric characterizations.

The centerlines of the segmented lumens were generated automatically using VMTK's Voronoi-diagram-based approach (Antiga *et al.*, 2008), which also provides local measurements of the maximally-inscribed sphere radius (i.e., minimum radius). In order to truncate the CCA centerline at an objective location proximal to the bifurcation, we used VMTK's definition of a bifurcation coordinate system and distances based on lumen radii (Antiga and Steinman, 2004). Specifically, the CCA was truncated one lumen radius proximal to where the CCA splits into the ICA and ECA, a point referred to as CCA1 (Hoi *et al.*, 2010a). These centerline trajectories and lumen radii were then used exclusively for subsequent geometric characterizations.

As the CEMRA acquisitions, and hence the segmented lumens, were oriented to the body axes, the total axial length of the CCA could be calculated as the distance along the superior-inferior axis between the thorax origin and CCA1, points hereafter referred to as T and C, respectively. As shown in Figure 1b for a representative case, each CCA was divided into nominal cervical and thoracic segments at the point of maximum curvature (called the pivot point, or P) between 50–70% of the total CCA length, L. For each of the cervical and thoracic segments a plane was fitted using a least-squares approach. After projecting each segment onto its respective plane, a best-fit circular arc (Figure 1c) was used to characterize the segment's mean radius of curvature (RC). Also noted was the mean segment lumen radius; the straight-line distances (SLD) from the respective arc end points; and the root-mean-square (RMS) deviation of the original centerline segments from their respective best-fit planes, as an estimate of segment non-planarity. The cervical and thoracic planes were each defined by their normal and tangent vectors, the latter based on the directions of the respective SLD. The relative orientation of these two best-fit planes was characterized by two angles: the *tilt*, calculated from the dot product of the two tangent vectors; and the *twist*, calculated from the dot product of the two normal vectors.

2.3. Parametric Models and Computational Fluid Dynamics

As illustrated in Figure 1d, idealized models of any specific or statistical CCA could be constructed from the above-defined geometric parameters as follows. First, each of the planar cervical or thoracic arc segments was sampled at the arc end point, the arc middle point, and a point halfway between them. Then, these 6 points, plus the original pivot point, were spline-fitted in order to define a new centerline. Finally, the lumen cross-section was assumed to be circular with a radius equal to the average or nominal radius of the cervical segment.

CFD simulations of pulsatile flow in such parametric models of the CCA were carried out using a well-validated in-house solver (Ethier *et al.*, 1999; Minev and Ethier, 1999; Ethier *et al.*, 2000). Quadratic tetrahedral-element meshes were generated by ICEM-CFD (ANSYS, Inc., Canonsburg, PA) with node spacing of 0.3 mm, shown to be sufficient for resolving the velocity profiles (Manbachi, 2010). Fully-developed pulsatile (i.e., Womersley) inlet velocity boundary conditions were prescribed using a representative older adult flow rate waveform (Hoi *et al.*, 2010b). Traction-free boundary conditions were prescribed at the outlet. Rigid walls and constant blood viscosity of 0.035 cm^2/s were assumed. Based on the typical flow and heart rates at the CCA (Hoi *et al.*, 2010b), Reynolds (Re) and Womersley numbers were rounded broadly to values of 500 and 3, respectively.

2.4. Statistical Analyses

Paired Student's t-tests were used to test the significance of left vs. right and cervical vs. thoracic differences. Linear regression was performed to test for an effect of age on the various geometric parameters. In all cases significance was assumed for $P<0.05$.

While most of the geometric characterization is completely automated and hence perfectly reproducible in theory, it does depend on the segmented lumen surface, which is extracted with some operator intervention, and hence is a potential source of uncertainty. To quantify this, 7 left/right pairs (i.e., 14 cases) selected by random number generator were re segmented after 12 months and put through the same automated geometric analysis. Operator reproducibility was quantified using the intraclass correlation coefficient, where ICC>0.75 was considered excellent. Statistical analyses were performed using Prism v4.0c (GraphPad Software, La Jolla, CA).

3. Results

3.1. Shape Characterization

As tabulated in Table 1, the mean axial length of the left CCA was roughly 10 cm, significantly longer than the 8 cm right CCA. The diameter of the right CCA was significantly larger, by about 6%, than the left. Pooling left and right sides together, the CCA diameter was 5.0 mm.

The mean radius of curvature of the pooled left and right cervical CCA was 127 mm, significantly ($P<0.0001$) less curved than the thoracic CCA (pooled radius of curvature = 42 mm). As summarized in Table 1, and also shown in Figure 2, the right thoracic CCA was significantly more curved than the left. For the left CCA the mean radius of curvature of the pivot point was 43 mm, not significantly different than that for the thoracic segment (47 mm). For the right CCA, however, the pivot (mean radius of curvature = 57 mm) was significantly less curved than the thoracic segment (mean radius of curvature = 37 mm). These relationships were preserved after normalizing individual radii of curvature by individual lumen radii. For example, the pooled left and right lumen:curvature radius ratios for the cervical vs. thoracic CCA were 1:50.1 vs. 1:16.3 ($p<0.0001$); and the right thoracic CCA was significantly more curved than the left (1:14.2 vs. 1:19.0; $p = 0.0145$).

The plane of thoracic curvature was tilted from that of cervical curvature by 23°, not significantly different between left and right sides. The left and right twist angles were, however, significantly different. Both were closer to 90°, reflecting the non-planarity of the CCA geometry. RMS deviations from the planes of curvature were significantly higher on the left side for both cervical (0.56 vs. 0.27 mm; $p = 0.032$) and thoracic (0.59 vs. 0.35 mm; $p = 0.001$) segments; however, there was no significant difference between cervical and thoracic RMS deviations.

As shown in Table 2, there was a weak but significant or near-significant effect of age on certain geometric parameters, notably those related to CCA tortuosity such as curvature, RMS and tilt angle. As summarized in Table 3, excellent reproducibility was found for all key geometric parameters except twist angle, for which reproducibility was still acceptable at ICC = 0.61.

3.2. CFD Models

A parametric model of a "typical" CCA was constructed from the following median values, suitably rounded: 1:60 cervical lumen:curvature radius ratio; 1:15 thoracic curvature; 60 mm and 40 mm cervical and thoracic SLD; 25 and 90 degree tilt and twist; and 5-mm diameter. To investigate the effect of thoracic curvature, additional models were constructed using 1:45 and 1:10 thoracic curvatures, representing 10^{th} and 90^{th} percentile curvatures, with all other parameters fixed. These models, along with a 1:60 cervical-only model, are shown in Figure 3.

Figures 3a and 3b summarize the complex, time-averaged wall shear stress (WSS) and flow patterns present in the median model of a "typical", albeit idealized, CCA with thoracic curvature ratio of 1:15. This modestly curved thoracic segment introduces strong velocity profile skewing and WSS asymmetry into the cervical segment, which, due to the relative tilt and twist, causes the velocity profile, and hence regions of high vs. low WSS, to rotate nearly to the opposite wall. Although progressively damped by the more shallow curvature of the cervical segment, pronounced velocity profile skewing and elevated WSS towards the outer wall of the cervical bend is still evident near the model outlet. Inspection of the 10^{th} and 90^{th} percentile (1:45 and 1:10) models reveals that thoracic velocity profile skewing increases with thoracic curvature as expected; however, the degree and orientation of skewing downstream in the cervical segment appears largely independent of upstream thoracic curvature. Interestingly, velocity profile skewing is strongest for the case of an isolated (planar) cervical segment.

These findings are echoed in Figure 3c, which reveals patterns of in-plane (secondary) flow at the outlet, which, for models with a thoracic segment, are dominated by a clockwise vortex offset from the center. A smaller, counter-clockwise vortex is evident for the 1:15 case and, to a lesser extent, the 1:10 case. On the other hand, the cervical-only case shows symmetric, counter-clockwise secondary flow structures consistent with Dean-type flow in a planar bend (Berger *et al.*, 1983). Maximum secondary velocity magnitudes at the outlets were 13%, 12% and 15% of the mean axial velocities for the 1:10, 1:15 and 1:45 cases, respectively, but just 7% for the cervical-only case. Average secondary velocities at the outlet were roughly half of the peak values. Velocity profile skewing and secondary velocities were obviously stronger at the pivot point, with peak values of the latter being approximately double those at the corresponding outlets.

4. Discussion

4.1. Summary and implications of findings

The present study characterizes, apparently for the first time, the complete shape of the adult human common carotid artery in vivo, and illustrates its impact on velocity profile skewing. These data fill an important gap left by previous studies, which have relied on the implicit or explicit assumption that the CCA can be considered long enough and straight enough to justify fully developed flow. In particular, our observation of non-negligible velocity profile skewing for median curvatures of the cervical CCA is consistent with Ford et al.'s (2008) assertion that fully-developed flow in the CCA is "the exception rather than the rule".

That a seemingly shallow median lumen:curvature radius ratio of 1:60 is sufficient to produce flow patterns that so strongly violate the Poiseuille flow assumption may seem surprising at first. However, consider that the degree of velocity profile skewing scales with the dimensionless Dean number, De, which reflects the ratio of centrifugal to viscous forces. In its recommended form – the definition of De unfortunately varies widely (Berger *et al.*, 1983) – the Dean number is the product of the Reynolds number (based on lumen diameter) and the square root of the lumen:curvature radius ratio. In the present CFD simulations, with a time-averaged Re = 500, De = 65, a value that would be expected to cause non-negligible velocity profile skewing (Berger *et al.*, 1983).

As might be expected from the anatomical constraints, the thoracic CCA segment was significantly more curved than the cervical segment; however, the degree of thoracic curvature had only a modest impact on the nature of the velocity profile by the time it approached the (absent) carotid bifurcation, at least compared to the case with no thoracic segment. Moreover, there was no obvious trend between the degree (or absence) of thoracic curvature and the outlet axial or secondary velocity characteristics. Some of this may be attributed to the lack of fine control of curvature in these parametric models: for the 1:10, 1:15 and 1:45 thoracic curvature cases, the mean cervical curvature (nominally 1:60) was higher (1:51, 1:57, 1:54, respectively) owing to the need to accommodate a natural curvature at the pivot. Nevertheless, despite these stronger mean cervical curvatures, and hence up to 10% higher cervical Dean numbers, it was the 1:60 cervical-only case that had the strongest velocity profile skewing. The pivot curvature was also variable for these cases (1:27, 1:30, 1:40, respectively), consistent with the range of pivot curvatures reported in Figure 2 yet, again, there was no obvious trend between thoracic/pivot curvature and pivot velocity profile characteristics. These findings highlight the complexity of the interactions between compound curvatures and the flow patterns within. In general, however, the compound nature of these curvatures produced secondary flows in the cervical CCA that were dominated by a single, or at least dominant, vortex, namely spiral flow consistent with that observed in vivo (Stonebridge *et al.*, 1996) or simulated in models of the femoral arteries (Wood *et al.*, 2006). In this context it is worth noting that the case with no thoracic segment produced the strongest velocity profile skewing, with weaker, counter-rotating secondary flows. Such persistent influence of thoracic velocities on the nature of flow well into the cervical segment is broadly consistent with the notion of a beneficial “morphodynamic” effect of asymmetry on flow inertia (Kilner *et al.*, 2000). Taken together, these findings suggest that models of the CCA (or indeed any artery) based on a single planar bend (e.g., Balbis *et al.*, 2005; Krams *et al.*, 2005; Leguy *et al.*, 2009) rather than compound curvatures might over- and underestimate velocity profile skewing and secondary velocities, respectively.

Returning to the main finding of our study, the presence of skewed velocity profiles was demonstrated in a model CCA representing a typical geometry that might be encountered clinically, insofar as it was derived from measurements of older adults recruited from a large, community-based study. This reinforces questions that have been raised about the reliability of clinical measurements of flow and wall shear rates, which tend to rely on simplistic assumptions about the velocity profile shape (Pantos *et al.*, 2007). For example, in Doppler ultrasound it is straightforward to measure, along the beam direction, the maximum blood velocity within a given artery cross-section. Under the assumption of negligible secondary flow, this maximum velocity can be projected onto the direction of nominal axial flow. A mean cross-sectional velocity can then be calculated as one-half of the peak velocity under the assumption of a parabolic (i.e., Poiseuille) velocity profile, allowing flow or wall shear rates to be readily estimated. Model studies using idealized curved tube geometries have demonstrated errors of up to 25% when estimating flow using the Poiseuille flow assumption (Krams *et al.*, 2005). Improvements may be possible using model-based

approaches that presume the kind of Dean-type velocity profile associated with flow in a planar bend (Verkaik *et al.*, 2009); however, it remains to be seen how well these work for non-ideally skewed velocity profiles characteristic of spiral flows reported here.

Finally, vascular wall remodeling is thought to be mediated by vascular wall shear stress, and so if WSS is not circumferentially uniform, then remodeling may not be either. The CFD models in Figure 3a show that TAWSS near the outlet varies from about 0.75 to 2.25 times the nominal inlet value, namely a threefold circumferential variation. This might help explain the common finding of eccentric rather than axisymmetric wall thickening at the proximal CCA (Boussel *et al.*, 2007). On the other hand, our findings are unlikely to have implications for understanding the development of atherosclerotic lesions at the carotid bifurcation, insofar as recent work from our group suggests that "memory" of the incoming CCA velocity profile is effectively lost as it enters the geometrically-dominating bifurcation region (Hoi *et al.*, 2010a).

4.2. Relationship to previous work

Our finding that parameters related to the curvature and relative orientation of the CCA segments tend to increase with age is broadly consistent with the well-known effect of age on tortuosity (Wenn and Newman, 1990); however, few studies have attempted to quantify the nature of such tortuosity or curvature. An early case study by Caro et al. (1992) reported a lumen:curvature radius ratio of 1:20 from sagittal magnetic resonance angiograms of a "healthy volunteer" (age unknown), and noted the presence of Dean-type velocity profiles in axial scans. This relative curvature is close to the maximum found in the present study (1:18); however, the authors noted that when "the subject's head was raised a few inches with a cushion" in a subsequent scan, the CCA appeared straight and velocity profiles were much more axisymmetric. Nevertheless, based on their assumed Reynolds number of 300 those authors estimated a Dean number of 60, comparable to that used for our median CCA models.

More recently, Tortoli et al. (2003) reported that "rough estimates of the radius of curvature were always in the range of 10 to 40 cm" based on longitudinal B-mode or MRI scans of "20 healthy volunteers, with ages of between 26 and 88 years". These values compare favourably with the range of cervical curvatures reported in our Table 1. In vitro investigations of planar curved tubes with De = 61 (based on their specific Re = 500 and 1:67 curvature ratio) showed evidence of "M-shaped" velocity profiles characteristic of strong velocity profile skewing, whereas a curvature of 1:100 showed more modest skewing. Those authors also noted from one of their in vivo studies that in one longitudinal view "the CCA looks like a straight vessel, in the second view it appears bent with an approximate curvature radius of 30 cm." This is consistent with our finding that the cervical carotid can typically be approximated as a planar curve. In their single case study, Caro et al. (1992) reported cervical curvature in the sagittal view, but not the coronal view. In our broader sample, 20 cases had a plane of cervical curvature within a span of 45° centered on the sagittal plane, compared to only 10 cases within the same proximity of the coronal plane; however, this leaves nearly half of the 56 cases having no obvious orientation relative to the body axes.

Where we did find disagreement with previous work was our mean CCA diameter of 5.0 mm, which was significantly lower than the 6.1–6.5 mm mean diameters reported from ultrasound imaging of comparably aged adults (e.g., Polak *et al.*, 1996; Samijo *et al.*, 1998; Jensen-Urstad *et al.*, 1999). To explain this apparent 20–30% underestimation, we note that our diameters were averaged along the length of the cervical CCA, whereas those previous measurements were made a few cm proximal to the carotid bifurcation flow divider. For example, at a location corresponding to 2 cm proximal to the flow divider we found a

significantly higher mean CCA diameter of 5.58 mm. Furthermore, our sample included a disproportionate number of females, who tend to have smaller CCA diameters (4.69 mm vs. 5.55 mm for males in our study). Rescaling to account for this increased our mean diameter by a further 2.4%. This leaves a 7–14% underestimation of CCA diameters and, consequently, lumen:curvature radius ratios. An obvious suspect would be partial volume blurring of the lumen boundaries owing to the 0.8–1 mm spatial resolutions of the CEMRA; however, even assuming a 5-mm diameter this was well above the three-pixel-per-diameter threshold suggested by Hoogeveen *et al.* (1998) for accurate diameter measurements. Instead, the likely culprit is our edge-based segmentation criterion, which does not account for the rounding of the lumen signal intensity profiles known to occur with centric CEMRA (Westenberg *et al.*, 2000). Nevertheless, this was expected to have a negligible effect on conclusions drawn from our CFD models of a typical CCA, insofar as the Dean number is proportional to the square root of the diameter, hence errors in De of only 3–7%; and, if anything, our models would be underestimating rather than overestimating secondary flow and velocity profile skewing.

4.3. Potential Limitations

The present study elected to rely on non-anatomic criteria to distinguish nominal cervical and thoracic segments after observing that the CCA typically, but not always, comprised three main curved segments. From a fluid mechanical point of view it might have been preferable to divide the CCA at points of minimum curvature or maximum torsion; however, while this may work well for frank curvatures such as those of the distal ICA (Piccinelli *et al.*, 2011), we found it difficult to unambiguously identify these features for the more subtle curvatures of the CCA. As a consequence of dividing the CCA at a point of maximum curvature, our spline-based parametric modeling approach, which is based on fitting to points sparsely sampled from planar circular arcs, produced segments that are not perfectly planar, as evidenced by the slight cervical “wiggles” in the 1:10 thoracic case and, to a lesser extent, the 1:15 case, in Figure 3b. These models also do not preserve the nominally constant curvature along the cervical segment, as can be seen by comparing the models with and without thoracic segments in Figure 3a. This was necessary in order to ensure physiologically smooth transitions between segments, and anyway these deviations are consistent with our finding of small but finite RMS deviations from curve planarity. Moreover, the agreement between the actual and approximated CCA geometries in Figure 1d supports this rational approach to the construction of anatomically plausible parametric models of the CCA.

Another consequence of our approach is that nearly-straight or nearly-helical cervical CCA segments will not, by definition, have a well-defined plane of best-fit curvature. As a result, twist angles for such cases may be spurious. Indeed, we noted that the four repeat analyses showing differences in twist angle > 30° between the first and second analysis had either low cervical curvature and RMS deviations (i.e., approximately straight), or high curvatures and deviations (i.e., approximately helical). This helps to explain why twist angle was the least reproducible of the geometric parameters, and suggests the need for a more robust approach to characterizing the transition between the nominal cervical and thoracic segments. Finally, and in light of our goal to characterize the shape of the CCA towards its influence on local hemodynamics, we made no attempt to define geometric parameters that were independent of one another. In fact, as might be expected, there were significant correlations ($P<0.01$) between tilt angle and cervical curvature; and between both tilt and twist angles and the cervical and thoracic RMS.

CFD simulations made the usual assumptions of a Newtonian viscosity and rigid walls. Non-Newtonian effects have been shown to be negligible for flow at the carotid bifurcation (Lee and Steinman, 2007), and so we expected the same to hold true for the simpler CCA

flows. Dis-tensions were expected to be less than ±10% over the cardiac cycle (Hansen *et al.*, 1995), and uniform over the length of the CCA, hence likely to have only a negligible effect on overall flow patterns. Where compliance might have an effect, however, is in the attenuation or dispersion of the flow pulse as it propagates along the CCA, whereas the present rigid model presumed the same flow pulse at the inlet and outlet. At the CFD model inlets we also assumed fully developed velocity profiles, whereas it is likely that the flow entering the thoracic CCA is strongly skewed as it comes off the aortic arch or brachiocephalic artery. That said, given the demonstrated minor influence of thoracic curvature on the cervical flow patterns, this might have only a minor effect on cervical CCA flow patterns. Finally, our parametric models assumed a constant diameter, whereas we showed that the diameter near the outlet is 12% greater than the diameter averaged along the cervical CCA. We did observe tapering along the CCA in most cases; however, this was difficult to quantify below the pivot point, since poorer signal-to-noise in the thoracic regions of the images tended to bias the minimum radius values downwards. Nevertheless, since the aim of the study was to demonstrate the effect of certain geometric parameters on gross velocity profile shapes, none of these limitations would likely impact its conclusions. The same may not be true, however, for more quantitative analyses, say aiming to predict the degree of velocity profile skewing from CCA curvature or vice-versa.

5. Conclusion

The typical human CCA possesses a modest but complex, three-dimensional curvature that belies the assumption it is “straight enough” to harbor fully-developed, axisymmetric blood flow. While this may not have a significant effect on flow patterns and hence plaque formation at the carotid bulb, owing to the dominating influence of carotid bifurcation geometry, it may help explain eccentric wall thickening often found at the proximal CCA. More importantly, our study reinforces concerns about the accuracy of clinical measurements that rely on simplistic assumptions about velocity profile shape, whether at the CCA or other nominally straight vessels that possess similarly modest curvatures. Further understanding of the role of compound curvature in flow and mass transport may also help inform the design of engineered arterial conduits (e.g., Huijbregts *et al.*, 2007).

Acknowledgments

This work is supported by a grant to DAS from the Heart & Stroke Foundation of Canada. DAS and YH also acknowledge the support of a Career Investigator Award and a Research Fellowship, respectively, from that agency. The VALIDATE study is supported by Contract NO1-AG-3-1003 from the National Institute on Aging, and, in part, by the Intramural Research Program of the NIH, National Institute on Aging.

References

Antiga L, Piccinelli M, Botti L, Ene-Iordache B, Remuzzi A, Steinman DA. An image-based modeling framework for patient-specific computational hemodynamics. Med Biol Eng Comput. 2008; 46:1097–112. [PubMed: 19002516]

Antiga L, Steinman DA. Robust and objective decomposition and mapping of bifurcating vessels. IEEE Trans Med Imaging. 2004; 23:704–13. [PubMed: 15191145]

Balbis S, Roatta S, Guiot C. Curvature affects Doppler investigation of vessels: implications for clinical practice. Ultrasound Med Biol. 2005; 31:65–77. [PubMed: 15653232]

Berger SA, Talbot L, Yao L-S. Flow in curved tubes. Annu Rev Fluid Mech. 1983; 15:461–512.

Boussel L, Serusclat A, Skilton MR, Vincent F, Bernard S, Moulin P, Saloner D, Douek PC. The reliability of high resolution MRI in the measurement of early stage carotid wall thickening. J Cardiovasc Magn Reson. 2007; 9:771–6. [PubMed: 17891614]

Carallo C, Irace C, Pujia A, De Franceschi MS, Crescenzo A, Motti C, Cortese C, Mattioli PL, Gnasso A. Evaluation of common carotid hemodynamic forces. Relations with wall thickening. Hypertension. 1999; 34:217–21. [PubMed: 10454444]

Caro CG, Dumoulin CL, Graham JM, Parker KH, Souza SP. Secondary flow in the human common carotid artery imaged by MR angiography. J Biomech Eng. 1992; 114:147–9. [PubMed: 1491578]

Ethier CR, Prakash S, Steinman DA, Leask RL, Couch GG, Ojha M. Steady flow separation patterns in a 45 degree junction. J Fluid Mech. 2000; 411:1–38.

Ethier, CR.; Steinman, DA.; Ojha, M. Comparisons between computational hemodynamics, photochromic dye flow visualization and magnetic resonance velocimetry. In: Xu, XY.; Collins, MW., editors. The haemodynamics of arterial organs - comparison of computational predictions with in vivo and in vitro data. WIT Press; Southampton: 1999. p. 131-83.

Ferrucci L. The Baltimore Longitudinal Study of Aging (BLSA): a 50-year-long journey and plans for the future. J Gerontol A Biol Sci Med Sci. 2008; 63:1416–9. [PubMed: 19126858]

Ford MD, Xie J, Wasserman BA, Steinman DA. Is flow in the common carotid artery fully developed? Physiol Meas. 2008; 29:1335–49. [PubMed: 18854602]

Giddens DP, Zarins CK, Glagov S. The role of fluid mechanics in the localization and detection of atherosclerosis. J Biomech Eng. 1993; 115:588–94. [PubMed: 8302046]

Hansen F, Mangell P, Sonesson B, Lanne T. Diameter and compliance in the human common carotid artery--variations with age and sex. Ultrasound Med Biol. 1995; 21:1–9. [PubMed: 7754568]

Hoi Y, Wasserman BA, Lakatta EG, Steinman DA. Effect of common carotid artery inlet length on normal carotid bifurcation hemodynamics. J Biomech Eng. 2010a; 132:121008. [PubMed: 21142322]

Hoi Y, Wasserman BA, Xie YJ, Najjar SS, Ferruci L, Lakatta EG, Gerstenblith G, Steinman DA. Characterization of volumetric flow rate waveforms at the carotid bifurcations of older adults. Physiol Meas. 2010b; 31:291–302. [PubMed: 20086276]

Hoogeveen RM, Bakker CJ, Viergever MA. Limits to the accuracy of vessel diameter measurement in MR angiography. J Magn Reson Imaging. 1998; 8:1228–35. [PubMed: 9848733]

Huijbregts HJ, Blankestijn PJ, Caro CG, Cheshire NJ, Hoedt MT, Tutein Nolthenius RP, Moll FL. A helical PTFE arteriovenous access graft to swirl flow across the distal anastomosis: results of a preliminary clinical study. Eur J Vasc Endovasc Surg. 2007; 33:472–5. [PubMed: 17161962]

Jensen-Urstad K, Jensen-Urstad M, Johansson J. Carotid artery diameter correlates with risk factors for cardiovascular disease in a population of 55-year-old subjects. Stroke. 1999; 30:1572–6. [PubMed: 10436103]

Kilner PJ, Yang GZ, Wilkes AJ, Mohiaddin RH, Firmin DN, Yacoub MH. Asymmetric redirection of flow through the heart. Nature. 2000; 404:759–61. [PubMed: 10783888]

Krams R, Bambi G, Guidi F, Helderman F, van der Steen AF, Tortoli P. Effect of vessel curvature on Doppler derived velocity profiles and fluid flow. Ultrasound Med Biol. 2005; 31:663–71. [PubMed: 15866416]

Lee SW, Steinman DA. On the relative importance of rheology for image-based CFD models of the carotid bifurcation. J Biomech Eng. 2007; 129:273–8. [PubMed: 17408332]

Leguy CA, Bosboom EM, Hoeks AP, van de Vosse FN. Assessment of blood volume flow in slightly curved arteries from a single velocity profile. J Biomech. 2009; 42:1664–72. [PubMed: 19481210]

Manbachi, A. Mechanical & Industrial Engineering. University of Toronto; Toronto: 2010. Characterization of common carotid artery geometry and its impact on velocity profile shape.

Minev PD, Ethier CR. A characteristic/finite element algorithm for the 3-D Navier-Stokes equations using unstructured grids. Comput Meth Appl Mech Eng. 1999; 178:39–50.

Pantos J, Efstathopoulos E, Katritsis DG. Vascular wall shear stress in clinical practice. Curr Vasc Pharmacol. 2007; 5:113–9. [PubMed: 17430215]

Piccinelli M, Bacigaluppi S, Boccardi E, Ene-Iordache B, Remuzzi A, Veneziani A, Antiga L. Geometry of the ICA and recurrent patterns in location, orientation and rupture status of lateral aneurysms: an image-based computational study. Neurosurgery. 2011

Polak JF, Kronmal RA, Tell GS, O'Leary DH, Savage PJ, Gardin JM, Rutan GH, Borhani NO. Compensatory increase in common carotid artery diameter. Relation to blood pressure and artery

intima-media thickness in older adults. Cardiovascular Health Study. Stroke. 1996; 27:2012–5. [PubMed: 8898807]

Samijo SK, Willigers JM, Barkhuysen R, Kitslaar PJ, Reneman RS, Brands PJ, Hoeks AP. Wall shear stress in the human common carotid artery as function of age and gender. Cardiovasc Res. 1998; 39:515–22. [PubMed: 9798536]

Stonebridge PA, Hoskins PR, Allan PL, Belch JF. Spiral laminar flow in vivo. Clin Sci (Lond). 1996; 91:17–21. [PubMed: 8774255]

Sui B, Gao P, Lin Y, Gao B, Liu L, An J. Assessment of wall shear stress in the common carotid artery of healthy subjects using 3.0-tesla magnetic resonance. Acta Radiol. 2008; 49:442–9. [PubMed: 18415789]

Tortoli P, Michelassi V, Bambi G, Guidi F, Righi D. Interaction between secondary velocities, flow pulsation and vessel morphology in the common carotid artery. Ultrasound Med Biol. 2003; 29:407–15. [PubMed: 12706192]

Verkaik AC, Beulen B, Bogaerds ACB, Rutten MCM, van de Vosse FN. Estimation of volume flow in curved tubes based on analytical and computational analysis of axial velocity profiles. Phys Fluids. 2009; 21:023602.

Wenn CM, Newman DL. Arterial tortuosity. Australas Phys Eng Sci Med. 1990; 13:67–70. [PubMed: 2375702]

Westenberg JJ, van der Geest RJ, Wasser MN, van der Linden EL, van Walsum T, van Assen HC, de Roos A, Vanderschoot J, Reiber JH. Vessel diameter measurements in gadolinium contrast-enhanced three-dimensional MRA of peripheral arteries. Magn Reson Imaging. 2000; 18:13–22. [PubMed: 10642098]

Wood NB, Zhao SZ, Zambanini A, Jackson M, Gedroyc W, Thom SA, Hughes AD, Xu XY. Curvature and tortuosity of the superficial femoral artery: a possible risk factor for peripheral arterial disease. J Appl Physiol. 2006; 101:1412–8. [PubMed: 16825527]

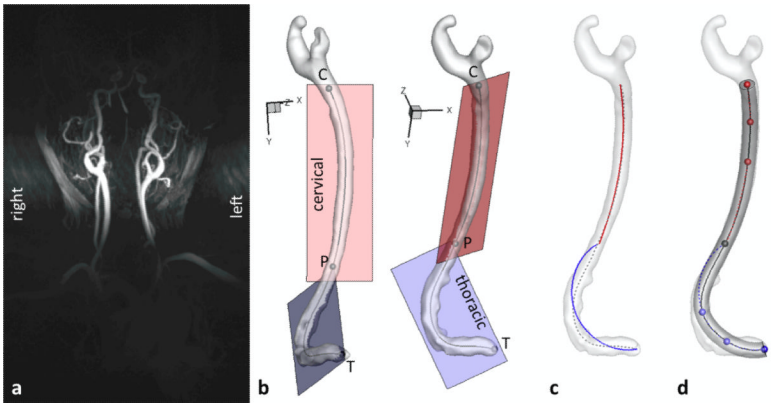

Figure 1.
(a) Maximum intensity projection of a representative 3D CEMRA. (b) Segmented right CCA viewed normal to best-fit cervical (left) and thoracic (right) planes. Note centerlines, pivot (P) and cervical (C) and thoracic (T) end points. (c) Best fit cervical and thoracic circular arcs (solid lines) compared to original centerline (dottedline). (d) Parametric CCA model derived from a spline fit of the indicated circular arc and pivot points, showing good agreement with the original CCA segmented surface.

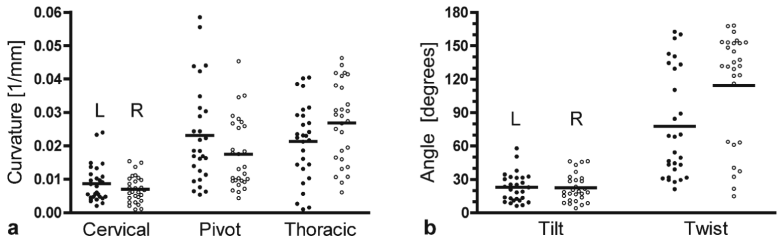

Figure 2.

Scatter plots of (a) curvature and (b) angle measurements from left (closed circles) and right (open circles) CCAs of 28 individuals. Horizontal lines indicate mean values.

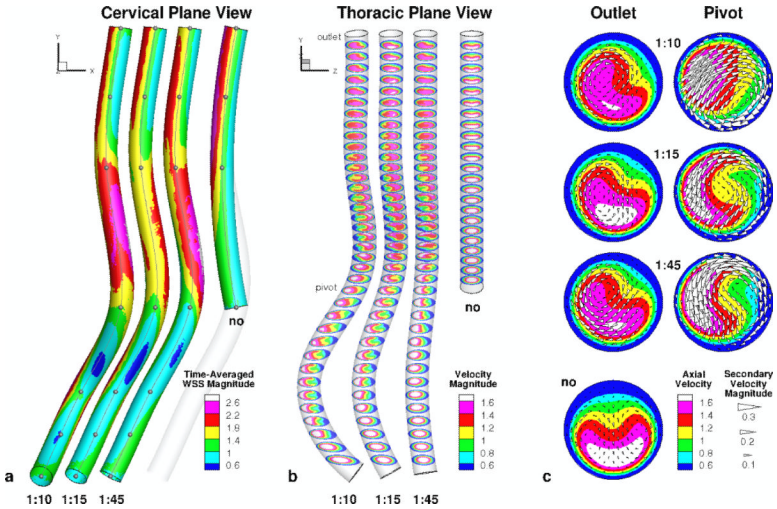

Figure 3.

Parametric CCA models with 1:60 cervical curvature and 1:10, 1:15 and 1:45 thoracic curvatures, along with a model with no thoracic segment. (a) Time-averaged wall shear stress (TAWSS), viewed normal to the cervical plane of curvature. TAWSS is normalized to its inlet value, with levels indicated by the contour legend. Shown also are the feature points and spline-fit centerlines used to construct the models; the no-thoracic model is superimposed on the 1:45 thoracic case to demonstrate that cervical feature points are the same in all cases. (b) The same parametric models, rotated 90° and then tilted 25° so as to be viewed normal to the thoracic plane of curvature, showing CFD-computed time-averaged velocity magnitudes on axial (Y) planes spaced one radius apart. Velocities are normalized to the mean inlet velocity, with levels indicated by the contour legend. (c) Time-averaged through-plane (axial) velocity contours and in-plane (secondary) velocity vectors from planes at the outlet and pivot points, with respective legends indicated.

Table 1

Descriptive statistics for CCA geometry, derived from left and right arteries segmented from CEMRA of 28 individuals.

	Dimensions (mm)				**Curvature (1/mm)**				**Transition (degrees)**			
	Length		**Diameter**		**Cervical**		**Thoracic**		**Tilt**		**Twist**	
	L	**R**	**L**	**R**	**L**	**R**	**L**	**R**	**L**	**R**	**L**	**R**
Mean	99.8	80.3	4.85	5.15	1/115	1/141	1/46.9	1/37.2	22.8	22.5	77.7	114.5
Stdev	10.8	10.7	0.79	0.85	1/178	1/250	1/87.1	1/83.7	13.0	12.6	48.2	49.5
Min.	79.9	58.4	3.48	3.54	1/487	1/1020	1/958	1/163	6.4	4.3	21.4	15.0
Max.	119.9	99.5	6.85	6.98	1/41.7	1/64.9	1/24.7	1/21.6	58.0	46.4	162.7	168.3
L vs. R	*P<0.0001*		*P=0.003*		*P=0.116*		*P=0.041*		*P=0.899*		*P=0.013*	

Table 2

Linear regressions of age vs. geometric parameters. Shown are the goodness of fit (R^2) and P-values indicating whether slopes are significantly non-zero.

	Left		Right	
Parameter	**R^2**	**P**	**R^2**	**P**
Axial Length	0.01	0.622	0.00	0.951
Cervical Diameter	0.09	0.107	0.22	0.011
Cervical Curvature	0.14	0.053	0.24	0.008
Thoracic Curvature	0.17	0.032	0.13	0.060
Cervical RMS	0.23	0.010	0.16	0.035
Thoracic RMS	0.12	0.068	0.09	0.126
Tilt Angle	0.29	0.003	0.18	0.021
Twist Angle	0.12	0.065	0.06	0.210

Table 3

Intraclass correlation coefficients (ICC) showing operator reproducibility for geometric parameters.

Parameter	ICC
Axial Length	0.89
Cervical Diameter	0.99
Cervical Curvature	0.80
Thoracic Curvature	0.94
Cervical RMS	0.88
Thoracic RMS	0.88
Tilt Angle	0.98
Twist Angle	0.61